Environmental Science Nano

Evanescent wave interaction with nanoparticles on optical fiber modulate side emission of germicidal ultraviolet light

Journal:	*Environmental Science: Nano*
Manuscript ID	EN-ART-02-2021-000199.R1
Article Type:	Paper

Environmental Significance

Light emitting diodes (LEDs) are emerging as a low-cost, low-energy usage nanotechnology capable of emitting germicidal wavelengths capable for disinfection in air, water or on surfaces. A challenge is how to deliver light from relatively small point-sources of emitted light from LEDs into areas with unique geometries, such as piping or narrow channels. As an alternative method for light delivery, side-emitting optical fibers (SEOFs) have been investigated in the fields of photocatalysis, disinfection processes (*e.g.*, using wavelengths from <250 nm to ~300 nm), and optical sensors. We previously showed these capable to inactivate bacteria in water and control biofilm growth on surfaces. In SEOFs, UV light (*e.g.*, from LEDs) enters one end of the optical fiber and then is radially side-emitted in the air or water by silica nanoparticles (NPs) on the fiber's surface as light propagates along the fiber. Light radiating from a source is composed of refracted light and electromagnetic radiation within optical fibers. In our prior work we suspected that decreasing the separation distance would result in higher UV-C light scattering[3] because particles near the surface use more evanescent wave energy. However, there is a paucity of information about the function relationship between separation distance and light side emission. Thus, herein we focus on filling this knowledge gap and hypothesize that controlling the separation distance is an effective strategy to make distribution of side-emitted UV-C light along a SEOF more uniform, and easier to design and integrate into systems where non-chemical disinfection is required.

Evanescent wave interaction with nanoparticles on optical fiber modulate side emission of germicidal ultraviolet light

Zhe Zhao[1], Mariana Lanzarini-Lopes[1], Emma Westerhoff[3], Xiangxing Long[1,2], Hojung Rho[1,5], Yuqiang Bi[1], Li Ling[4], Paul Westerhoff [1*]

[1] NSF Nanosystems Engineering Research Center for Nanotechnology-Enabled Water Treatment, School of Sustainable Engineering and the Built Environment, Ira A. Fulton Schools of Engineering, Arizona State University, Tempe, AZ 85287-3005, USA

[2] Biodesign Swette Center for Environmental Biotechnology, Arizona State University, Tempe, AZ 85287-5701, USA

[3] Olin College, Needham, MA 02492, USA

[4] Department of Civil and Environmental Engineering, Hong Kong University of Science and Technology, Hong Kong, China

[5] Department of Land, Water and Environment Research, Korea Institute of Civil Engineering and Building Technology, 283 Goyang-Daero, Ilsanseo-Gu, Goyang-Si, Gyeonggi-Do, 10223, Republic of Korea

*Corresponding author:

orcid ID: 0000-0002-9241-8759

Email: p.westerhoff@asu.edu

Phone: 480-965-2885

In preparation: *Environmental Science Nano*

Abstract

Silica nanoparticle coating on quartz optical fiber facilitates side-emission of germicidal ultraviolet light (UV-C), which shows promise for disinfection of contaminated air, water, and surfaces. However, the emitted light along the length of optical fibers decreases exponentially with distance from the LED light source, which makes designing applications more challenging and reduces overall useable length of optical fiber to disinfect water or surfaces. This work aims to develop an understanding of light interactions with the silica nanoparticles to allow more uniform side-emission of germicidal light along longer lengths of optical fibers. Two forms of light energy (refracted light and evanescent waves) are transmitted through optical fibers. The amount of side-emitted UV-C light is overwhelmingly controlled by the evanescent wave energy interacting with nanoparticles at distances from < 2 to 100 nm from the surface of the optical fiber. Varying the separation distance enables up to ten-fold (*10x*) modulation in intensity of side-emitted UV-C light, demonstrated 1) experimentally through ionic-strength modifications during a manufacturing process, and 2) through first-principle models. These insights enabled fabrication of side-emitting optical fibers (SEOFs) with more uniform light emission along their entire length (>30 cm). The fundamental insights and experimental validation into light interactions with nanoparticles on SEOF surfaces, in conjunction with prior bacterial inactivation studies, enables use of UV-C light produced by light emitting diodes (LEDs) to mitigate biofilm formation on confined surfaces commonly found in water treatment, premise plumbing, and cooling systems.

Introduction

Germicidal wavelengths from ultraviolet light emitting diodes (UV-C LEDs) is an emerging technology for disinfection of water and air. UV-C LEDs have several benefits over traditional low-pressure UV lamps or medium-pressure UV lamps: longer life span, mercury-free materials, targeted wavelength band, and lower direct current (DC) power requirements.[1, 2] However, LEDs are limited by their relatively small irradiation area and high attenuation of UV light in air and water, which reduces the area LEDs can disinfect microorganisms in air, water, or surface biofilms.[3, 4] To overcome these problems, complicated networks containing dozens or more LEDs are required to deliver germicidal light within reactors systems.[5] Additionally, many biofilms form in small diameter pipes, tubing, basins, and unit processes such as spiral wound membranes of water systems, and within biomedical (*e.g.*, endoscopes) or other devices (*e.g.*, washing machines) where conventional LED arrays cannot be easily installed. As such, a strategy is needed to deliver and distribute light from LEDs within such applications to achieve microbial disinfection and/or surface biofilm prevention.

As an alternative method for light delivery, side-emitting optical fibers (SEOFs) have been investigated in the fields of photocatalysis,[6, 7] disinfection processes (*e.g.*, using wavelengths from <250 nm to ~300 nm),[3, 8-10] and optical sensors.[11, 12] Commercial SEOFs could be obtained by micro-bending, fiber core doping or surface roughness.[13, 14] However, these methods only work well in visible spectrum due to the difficulty of silica material modification. We recently fabricated UV-C SEOFs utilizing silica sphere nanoparticles (NPs).[3] In UV-C SEOFs, UV light (*e.g.*, from LEDs) enters one end of the optical fiber and then is radially side-emitted in the air or water by silica NPs on the fiber's surface as light propagates along the fiber. The silica sphere

NPs, when coated on optical fibers, act as scattering centers to promote side emission of germicidal UV-C light for disinfection. Prior work showed that delivering at least 2 μW/cm^2 of 265 nm light from an optical fiber was sufficient to inhibit microbial activity on the UV-irradiated surfaces.[15] Compared with traditional UV light source configurations, SEOFs could increase irradiated surface area by connecting a single light source for efficient light delivery.[16, 17] Moreover, optical fibers with diameters < 1 mm are highly flexible and enable light to be delivered in small spaces. Key to achieving flexibility of these thin quartz fibers without compromising UV-C transmittance is a durable UV-C transparent polymer coating or cladding.[18] Such a polymer coating or cladding over the NPs also prevents losing them to solution.[3, 19] However, with all these benefits, when launching UV-C light from a LED into a SEOF, side-emitted light decays exponentially, *i.e.*, >90% of side-emitted light decays over 10-cm as light propagates along an optical fiber.[15] This limits the fabrication length of SEOFs. Shifting the distribution of side-emitted light along the length of a SEOF from an exponential to a more uniform distribution could enable longer fiber lengths that can deliver light to larger areas.

Light radiating from a source is composed of refracted light and electromagnetic radiation within optical fibers.[20] Solarized or high-OH quartz attenuates minimal UV-C light, with over 80% less attenuation compared to standard optical fibers.[21] When total internal reflection (TIR) occurs, an evanescent wave (*i.e.*, an electromagnetic wave generated at the side of the optically sparse medium) forms within the fiber.[22] This evanescent wave energy decays exponentially in a direction perpendicular to the outer surface plane of the fiber (illustrated in Figure 1). The separation distance (h) between NPs and the quartz fibers influences the amount of light energy scattered from the fiber.[23, 24] In our prior work we suspected that decreasing the separation

distance would result in higher UV-C light scattering[3] because particles near the surface use more evanescent wave energy. However, there is a paucity of information about the function relationship between separation distance and light side emission. Thus, herein we focus on filling this knowledge gap and hypothesize that controlling the separation distance is an effective strategy to make distribution of side-emitted UV-C light along a SEOF more uniform.

This paper explores how separation distances of <5 to 100 nm between silica NPs and optical fiber surfaces influence the amount of side-emitted UV-C light. First, experimental evidence showed that incorporating an ionic strength synthesis process into the SEOF fabrication compressed electric double layers, allowed tuning the electrostatic attachment distance between NPs and optical fiber surfaces, and achieved variable side-emitted light intensity. Experimental results were fitted to a single scattering efficiency (α) relationship. Second, a first-principle MATLAB model showed the relationship between separation distance (NPs to optical fiber), interactions with the evanescent wave energy in the optical fiber, and overall amount of side-emitted light from the optical fiber. Shorter separation distances led to higher intensities of side-emitted light. Third, we visually observed that increasing ionic strength treatments also led to more "patchy" NP coatings on the fiber surface, and the model provided insight into this phenomenon. Finally, the surface roughness and tuned separation distance accomplished by varying ionic strengths were used to design and synthesize SEOFs with improved uniformity of side-emitted light along the optical fiber length. The findings provide mechanistic insight into how NPs can be used to manage light within optical fibers. This information will help design the next generation of SEOFs for use in controlling biofilms in air and water treatment systems.

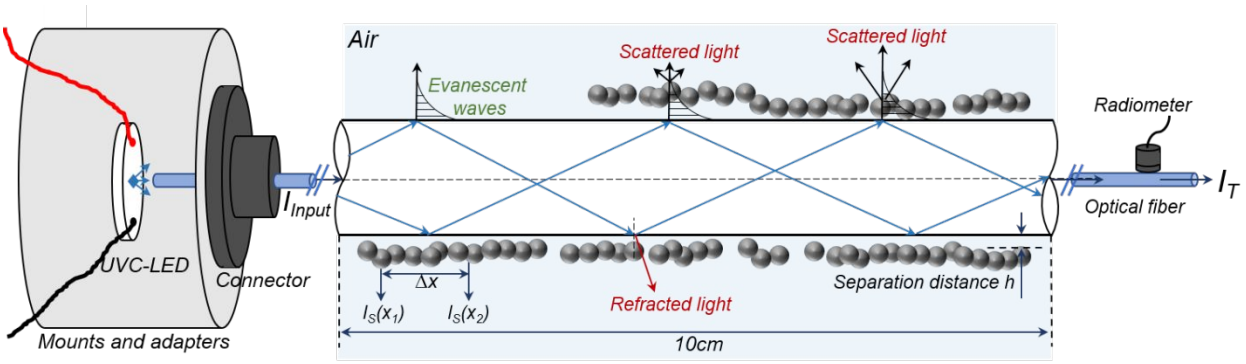

Figure 1 Schematic of the experimental setup with a 265 nm LED launching light through a SMA905 connector into a SEOF coated with silica nanoparticles and CyTop™ polymer along the entire fiber length. Blue insert section shows light rays (blue lines) propagating along an optical fiber from left (*i.e.*, light source) to the right (terminal end of the fiber). Illustrated as grey spheres, NPs attached near the fiber surface serve as scattering centers on the SEOF and interact with evanescent wave energy to side-emit light.

Methods and Materials

Fabrication of side-emitting optical fiber

Figure 1 depicts the UV-LED-SEOF system used in this study. Briefly, multimode optical fibers were purchased from Thorlabs (diameter of 1 mm, numerical aperture of 0.39, core refractive index (*RI*) of 1.5; FT1000UMT, High-OH for 300-1200 nm, Thorlabs, Newton, NJ). This high-OH fiber has >80% less attenuation compared to standard optical fibers. Figure SI.1 plots attenuation of 265 nm light up through a 1 meter section of this fiber. While light is clearly attenuated along the length of the fiber, there is still >20,000 μW/cm^2 of 265 nm energy available even at a length of 1 meter from the LED.

Protective cladding and coating materials on the as-received Thorlab fibers were first gently removed by a razor, and then the remaining impurities were dissolved by 95% acetone for 1 hour. The fiber was then cut into 10 cm lengths, and the cut surface on both ends was polished through 5 optical polish films (LF30D, LF5P, LF3P, LF1P, LF03P, Thorlabs, Newton, NJ) to obtain a smooth and clear surface. A fiber inspection scope (FS201, 200X, Thorlabs, Newton, NJ) was used to determine the uniformity of creak and clarity of the polished end. Then fibers were fixed to a 3 cm ferrule connector (SMO5SMA, 1020 um, Thorlabs) using heat shrink wrap, and heated air was used to shrink-wrap the assembly. A 60 mW 265 nm UV-C LED (KLARAN, NY) was mounted to polished fibers using a butt-coupling method of direct contact. A lens tube was used to decrease any potential light loss. To reduce the distance between the cut-end and LED, 2.5 mm length of stripped fiber was applied outside the connector.

Aminated silica sphere NPs (suspended in 99.99% ethanol, 10 mg/mL, nanoComposix, San Diego, CA) as scattering centers. As shown in Figure SI.2, high diameter NPs results in higher scattering, and scattering benefits plateaued for NP diameters above 200 nm. Therefore, as with prior work[3] we used 200 nm aminated silica sphere NPs as scattering centers. Nanoparticles were coated onto stripped optical fibers through electrostatic attractions. The fibers were dip-coated into aminated silica sphere nanoparticle suspensions for 60 seconds and dried in the air for 5 mins. This procedure was repeated twice to increase NP coverage to over 0.80 $\mu g/mm^2$ for a maximum side emission (Figure SI.3); additional layers (i.e., more dip-coating cycles) did not further increase side-emission of 265 nm light.

Transmission electron microscope (TEM; Philips CM 200) analysis was performed on the aminated nanoparticles to confirm particle size the manufacturer reported measurements. Silica nanoparticles dispersed in ethanol were added to a 200-mesh Au grid. 100 nanoparticles were counted for our size analysis. Particle size distribution pattern is shown in Figure SI.4. The range and distribution of silica NPs used in this work is 199 $\pm$ 5 nm, which confirmed the size and uniformity as reported by the manufacturer. Since side scattering of 265 nm light is not highly dependent ($p< 0.05$) upon NP diameters above 200 nm (e.g., Figure SI.2), the small variation in silica NP diameter (199 $\pm$ 5 nm) is unlikely to influence side scattering performance.

In order to manage the optical fiber scattering efficiency, the NP-coated optical fiber was submerged into variable aqueous ionic strength solution for 10 seconds and then dried for 5 min. A series of ionic strength concentrations (0.06 M, 0.15 M, 0.30 M, 0.45 M and 0.60 M) was prepared by Na_2SO_4 (Sigma-Aldrich, 244511). Note that this step could also be achieved by other salts (e.g., phosphates) that could change the solution ionic strength.[3] Each concentration was used separately to treat different optical fibers, and each concentration led to a different scattering coefficient (α). A 30 cm optical fiber was treated with different sodium sulfate concentrations every 6 cm to compare the uniformity to an untreated fiber. All figures report the average of triplicate results with standard deviation.

A low UV-C absorbing polymer (CyTop^{TM}, BELLEX International Corp, Wilmington, DE) was used to treat bare or NP-coated optical fibers. Fibers were dipped in the polymer solution and dried in the air for 2h. Control experiments (Figure SI.5) confirmed previous research[3] showing that CyTop^{TM} has negligible effects on attenuation, light scattering, and reflection.

Light measurements

The light emitted from the LED and entering the optical fiber (I_{Input}) can be either absorbed (I_{Abs}), scattered (I_S), or transmitted (I_T) and is described by the following equation:

$$I_{Input} = I_S + I_T + I_{Abs} \quad (1)$$

Light was measured by a spectrophotoradiometer (Avantes, Louisville, CO, AvaSpec-2048L, calibration: 200−1100 nm) at different lengths along the fiber (0, 2, 4, 6 and 8 cm) (Figure 1b). The spectrophotoradiometer tip touched the optical fiber surface at each measurement location to obtain the maximum flux (μW/cm^2). All measurements were performed triplicates.

Data processing and statistical analysis

Side-emitted light scattering and uniformity of SEOF were represented by a scattering coefficient (α) and uniformity coefficient (UC), respectively. Because the light distribution along the axial direction shows an exponential decay, α was obtained using following equation[25]:

$$\frac{I_S(x)}{I_{Input}} = e^{-\alpha \Delta x} \quad (2)$$

where $I_S(x)$ is the light intensity scattered at the length position x from the LED. From Eq. (2), the ratio of the light intensity at different positions along the axial length remains a fixed value and can be expressed as follow:

$$\alpha = \frac{-\ln \frac{I_s(x_2)}{I_s(x_1)}}{\Delta x} \quad (3)$$

where Δx is the distance between different locations, and $I_S(x_1)$ and $I_S(x_2)$ are the light intensity at different locations (Figure 1).

To develop a metric related to uniformity of light emission along the length of the fiber, a Uniformity Coefficient (UC), defined as the ratio of measured scattered light at two distances from the LED source, was calculated following this equation:

$$UC = \frac{I_{S,\,L=0.6L_T}}{I_{S,\,L=0.1L_T}} \quad (4)$$

where $I_{S,\,L=0.1L_T}$is the scattered light at a length along the fiber equivalent to 10% of the total fiber length (L_T), and $I_{S,\,L=0.6L_T}$is the scattered light at a length along the fiber equivalent to 60% of the total fiber length. The values of 0.1 L_T and 0.6 L_T were selected based upon their use in the water industry (*e.g.*, D_{10} and D_{60} ratios to represent gradation of sand particles in filters) and use to statistically represent skewness of distributions. UC range from zero to unity, with values closer to unity representing more uniformly distributed light along the fiber length. Our goal was to achieve UC > 0.5.

Nanoparticle coating and surface roughness measurements

Atomic force microscopy (AFM) was performed in Bruker Multimode 8 (Bruker, Santa Barbara, CA), and data were analyzed by a computer software (Nanoscope Analysis 1.9). The tip size was 4–10 nm, and all measurements were performed in a tapping mode with a 0.01–0.025 Ohm -cm antimony (n) doped Si cantilever, resonance frequencies of 320 kHz, and spring constant of 42 N/m. Quartz substrates were cut by a ceramic blade to a 1.5 cm×1.5 cm square and submerged in 99.9% acetone for 1h to remove any impurities. The substrate samples were prepared similar to SEOFs we used in this study. The clean quartz was dipped in 200 nm aminated silica sphere NP suspensions for 10 s (reduced from 60 s with the fibers to avoid any noise during scanning) and dried in the air for 5 min. Then half of the samples were treated with 0.2 M sodium sulfate for 10

s. Only dispersed particle images were used to determine the height difference between background and NP layers. All height measurements were performed in triplicate.

The surface roughness of uncoated and silica-coated fibers was determined by a ZeScope optical profilometer (Zygo ZeScope). Three fibers (5 cm length) were chosen: a bare optical fiber, a fiber coated with 200 nm silica nanospheres, and a 0.2 M Na_2SO_4-treated fiber coated with 200 nm silica nanospheres. A 50× objective combined with a 0.63× magnification changer was used for the optimum visualization of the 1 mm diameter optical fiber. A stitch of 5 × 3 images with a 20% overlap was used to increase the collection area, resulting in 100 μm × 140 μm 3D images for each measurement. At least three measurements were performed across the length of each fiber sample. The root mean square roughness R_{rms} of the surfaces was then reported to compare the surface roughness among samples.

Mechanistic model

A mathematical predictive model was developed and run in MATLAB version R2019b to generate light profiles ($\mu W/cm^2$) along the optical fiber length. Figure SI.6 shows the SEOF scattering efficiency model system diagram. Fiber parameters (length, diameter, material), NP parameters (size, density, placement), and system parameters (angle resolution, iterations, optional polymer coating, distance between radiometer and fiber) were input into the main file (Figure SI.7). Computational raytracing was used to calculate theoretical side-emission profiles. The light profile from the LED was divided into a series of small sections, and the ray was tracked along the fiber length, with trajectory and intensity governed by the laws of the model.

The radiation pattern is shown in Figure SI.8. Ratio of light entering to the fiber (R%) was calculated by integrating the LED radiation pattern with accepted angles:

$$R\% = \frac{2\int_0^{\theta_{crit}} \frac{1}{2} f_{LED}(\theta)^2 \, d\theta}{2\int_0^{\frac{\pi}{2}} \frac{1}{2} f_{LED}(\theta)^2 \, d\theta} \tag{5}$$

Three phenomena captured in the model include: 1) linear optics (Fresnel and Snell equations), which dictate the trajectory and intensity of the light reflecting inside the optical fiber; 2) evanescent waves, which occur when a ray hits the edge of the fiber where a nanoparticle exists; and 3) Mie scattering, which occurs when any amount of light interacts with a nanoparticle. The angle of refracted light and the light intensity inside the optical fiber was calculated by Snell's law and Fresnel equations:

$$\theta_t = \frac{n_1 \sin(\theta_i)}{n_2} \tag{6}$$

$$I = \frac{n_1 \cos(\theta_i) - n_2 \cos(\theta_t)}{n_1 \cos(\theta_i) + n_2 \cos(\theta_t)} \tag{7}$$

where θ_i represents the angle of incident light, θ_t represents the angle of refracted light, n_1 and n_2 represents the reflective index of two media, and I represents the light intensity inside the optical fiber. The Mie profiles for the particles were generated using MiePlot v4.6.14, which provides a simple interface to the classic BHMie algorithm[26] for Mie scattering from a sphere.

Results and Discussion

Varying nanoparticle separation distance from SEOF modulates the extent of UV-C side scattering

Based on our prior surface disinfection research,[15] a minimum intensity of 2 μW/cm^2 of side-emitted UV light at 265 nm was needed to mitigate growth of *Pseudomonas aeruginosa* or *Escherichia coli* on a nutrient-rich surface. Therefore, in this work we targeted 2 μW/cm^2 as the light intensity that should be achieved by the SEOF at any length along the fiber. Insufficient light scattering to achieve bacterial control (*i.e.*, < 2 μW/cm^2) was observed for bare fiber without any NP modification at any length along a 10 cm SEOF (Figure 2). However, attaching NP scatter centers on the optical fiber enabled side-emission of 265 nm light above the target of 2 μW/cm^2. As shown in Figure 2, for all SEOFs that included NP coatings, light intensities were greatest near the LED source (*i.e.*, fiber length (cm) closer to zero) and then exponentially decreased further from the LED source.

To experimentally study the effect of separation distances (*h*) between the optical fiber surface and NP (illustrated in Figure 1), the NP-coated fibers were sequentially immersed in different ionic strength solutions for 10s and allowed to air dry. Then a protective UV-C transparent polymer coating was applied to the modified fiber. As shown in Figure 2a-e, inclusion of the ionic strength treatment increased the side-emitted light at any length along the fiber by a factor of 2*x* to nearly 10*x*. This is consistent with previous work that showed ionic strength increases the side emission at midpoint of the SEOF.[3]

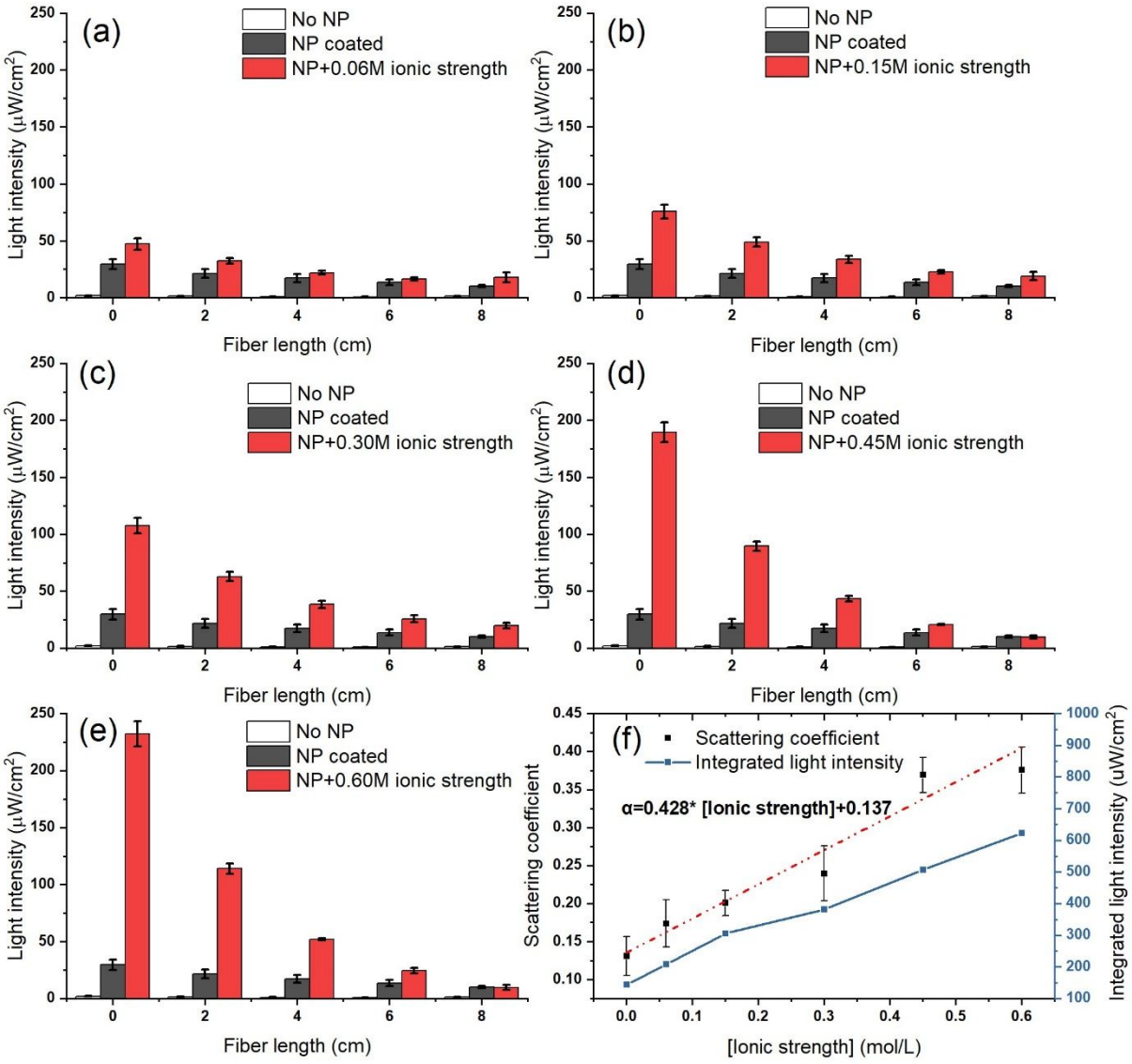

Figure 2 UV-C irradiance measured along the optical fiber length with ionic strength at (a) 0.06 M, (b) 0.15 M, (c) 0.30 M, (d) 0.45 M, and (e) 0.60 M; (f) linear fitting of scattering coefficient (left, dashed line) and integrated light intensity (right, solid line) with ionic strength used on SEOF. The standard deviations for triplicate independent optical fibers are illustrated as error bars.

SEOFs in Figure 2 show side-scattered light, but there was approximately 60% decrease of side-emitted light intensity from the proximal (L = 0 cm) towards the distal end without the ionic strength treatment and larger drops in side-emitted light intensity of 66%, 75%, 81%, 94%, and 96% when 0.06 M, 0.15 M, 0.30 M, 0.45 M, and 0.60 M ionic strength were applied, respectively. While the fibers are 10 cm in length, only light side-emitted along the first 8 cm was measured; at the very end (distal) of the fiber (L=10cm) light that was transmitted through the entire fiber is axially- (not side-) emitted. Along the fiber, more light is side-scattered from the SEOF near the LED source, thus is less light available to travel down the length of the fiber. The exponential light attenuation along the fiber confirms relatively uniform NP coating conditions along the fiber length. The exponential decreases in light along the fiber are, inherently, not uniform, as reflected by a decrease in UC (Equation 4) from 0.52 to 0.13 for a 10-cm optical fiber within the ionic strength range of 0-0.60 M (Table SI.2).

Scattering coefficients (α) were calculated using Equation 3 for each experiment (Supporting Information shows data fits, and Table SI.1 summarizes α values). Figure 2f shows that α were linearly correlated ($R^2 = 0.95$) with the ionic strength:

$$\alpha = 0.428 * [\text{Ionic strength, M}] + 0.137 \quad (8)$$

Additionally, Figure 2f shows the integrated light intensity (*i.e.*, total amount of side-emitted light along the entire fiber geometrically estimated based on measured point values) from the proximal (L = 0 cm) towards the distal end of the SEOF. Ionic strength of 0.06 M, 0.15 M, 0.30 M, 0.45 M, and 0.60 M led to increases of 1.4*x*, 2.1*x*, 2.6*x*, 3.5*x,* and 4.3*x* for the integrated light intensity relative to zero ionic strength treatment, respectively. As a control, optical fibers treated

only with ionic strength (no NP) showed zero side-emitted light, and therefore the side emission was not the result of salt crystals or other salt-related deposits (discussed more below). Overall, these experiments demonstrated side-scattering from NP-coated SEOFs depended on ionic strength (*i.e.*, Equation 8).

Separation distance determines the light distribution along the fiber

As shown in Figure 2, introducing ionic strength into SEOF synthesis could increase light scattering and modulate the scattering coefficient (α). Hence, we hypothesized that ionic strength would influence separation distance between the aminated silica NPs and the optical fiber quartz surface, thus increasing light scattering through greater interaction with the evanescent wave energy. However, it is difficult to measure the exact separation distance because the particles on the curved fiber surface usually overlap and are distributed unevenly, making it difficult to understand the effect of distance on light scattering. Typical separation distances are likely below 100 nm depending on the coating particle size.[27-30] To provide insights into the relative importance of separation distances on side emission of light from the fibers, we developed and used a MATLAB-based predictive model to simulate the effect of separation distance (0 to 100 nm) on the light scattering along optical fiber. Model conditions mirrored experimental conditions (*i.e.*, 200 nm particle size, 0.45A current with a 265 nm UV-C light with the emission profile provided by the manufacturer, optical fiber with a numerical aperture of 0.39, CyTop™ polymer coating).

Figure 3a shows simulated UV-C light irradiance at different distances along the optical fiber with separation distances (h) ranging from 1 nm to 100 nm between the NP and SEOF surface.

The model predicted an exponential decrease in side-emitted light and similar magnitudes of light intensity as observed in the experimental data (Figure 2). Figure 3b plots scattering coefficients calculated (Table SI.3) from data in Figure 3a. Figure 3b shows an exponential dependence of the scattering coefficient on the separation distance ($\alpha = 0.532\ e^{-0.048\,(h)}$; $R^2 = 0.997$). Using this relationship, the separation distance without ionic strength treatment is estimated to be approximately 30 nm. The separation distance reduced from 30 nm to approximately 5.5 nm when the ionic strength increased from 0 to 0.60 M (Equation 8). Overall, separation distances between 1 and 30 nm dramatically affected side-emitted light scattering.

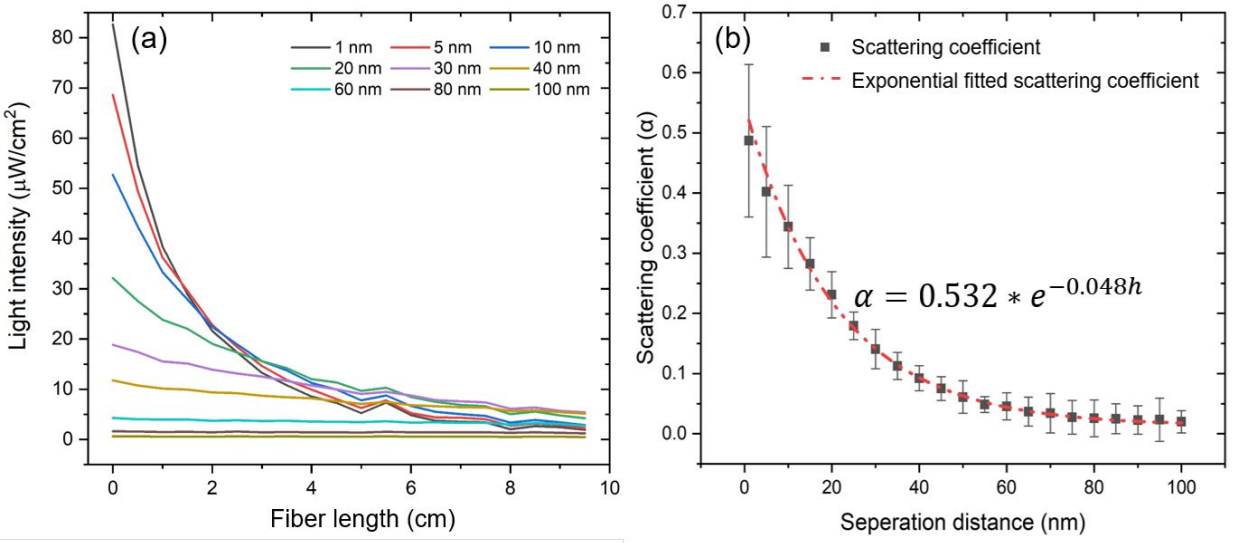

Figure 3 (a) Simulated UV-C light irradiance at different lengths along the optical fiber from the LED source (x=0) with separation distances ranging from 1 nm to 100 nm; (b) calculated average scattering coefficient along the fiber associated with the different scattering distances shown in Figure 3a. The standard deviations for the calculated scattering coefficient at different SEOF lengths are illustrated as error bars.

Our model incorporates two modes of interaction between light and NPs. The refractive light and evanescent waves on the surface both contribute to the divergence and transmission of light between different media. According to the Fresnel equation (Equation 7), light in the optical fiber would be refracted out of fiber interface when the external material's refractive index is either higher than or similar to the fiber material. When light in the optical fiber is completely reflected internally, the intensity at the interface between the two media will not suddenly become zero because the electric and magnetic fields cannot be discontinuous at a boundary.[30] Some light penetrates the surface and diffuses into the surrounding medium, thus an evanescent field is generated with a penetration depth that depends on the incident wavelength.[23, 31] Therefore, given a wave vector k, the evanescent wave field E(**r**) can be expressed according to Equation 10:

$$\boldsymbol{k} = k_y\hat{y} + k_x\boldsymbol{x} = i\alpha\hat{y} + \beta\boldsymbol{x} \tag{9}$$

$$E(\mathbf{r}) = E_0 e^{-i\,(i\alpha\hat{y} + \beta\boldsymbol{x})} = E_0 e^{(\alpha\hat{y} - i\beta\boldsymbol{x})} \tag{10}$$

This energy will spread and attenuate perpendicular to the interface (x-y plane). The intensity of this electric field in z direction can be described according to Equation 11:[17, 20]

$$I(h) = I_0 e^{-h\frac{4\pi\sqrt{n_f^2\sin^2\theta - n_2^2}}{\lambda}} \tag{11}$$

where n_f and n_2 are the reflective indexes of optical fiber and medium, respectively; I_0 is the maximum scattering intensity closest to the scattering center; h is the separation distance; and $I(h)$ is the scattering intensity at that distance. Therefore, the rapidly decaying energy field of evanescent wave highly depends on the distance from the fiber interface (h), which was determined by density of particle, density of medium, radius of particle, zeta potential of particles, and bulk ionic concentration.[32, 33] The evanescent wave intensity is higher in water (n_{water}= 1.33) than air (n_{air}= 1) due to the relatively high refractive index of water.

Following from Equation 11, for 265 nm incident light, the effective radial distance of evanescent wave on the fiber used in this study should be less than 100 nm (Figure SI.9). Therefore, loading NPs on the fiber will effectively influence *h* because ~30 nm separation distance is expected even without ionic strength treatment.

Figures 4a-c illustrate the mechanism of particle interaction with the evanescent waves at the fiber interface. With NPs on the optical fiber, the refractive index on each side of interface was similar (*RI*=1.5). Therefore, light emission is possible by refracting photons from the fiber waveguide into the NP layer and reacting with evanescent field near the fiber interface. Modulating *h* controls the electric field of the evanescent wave to increase light emission (Figure 4b and 4c). This understanding is consistent with Hideki's work that particle diffusion behavior could be monitored by the evanescent wave dynamic light scattering, and the diffusion behavior of a colloidal particle near the interface can be extracted quantitatively as a function of the distance from the interface.[34] Compared to the side-emitted light, the transmitted light accounts for over 90% of the energy within the entire fiber. Overall, our modelling showed that > 95% of side-emitted light was associated with interactions between the NP and evanescent waves.

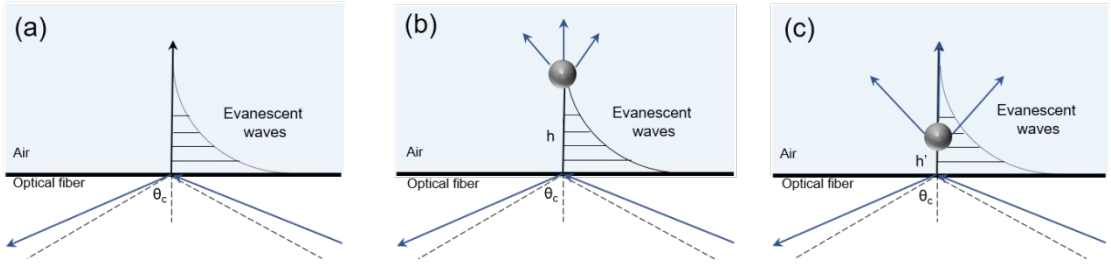

Figure 4 Schematic of evanescent wave - fiber interface interactions (a) without and (b, c) with NPs.

Influence of ionic strength treatments on separation distances and surface roughness

Modeling showed that separation distances of 0 to 30 nm influenced the amount of side-emitted light (*i.e.*, higher α with shorter distances). To quantify these parameters, AFM and optical profilometer measurements were performed. Figures 5a and 5b show AFM images of a flat quartz slide, which approximated the curved optical fiber, coated with NP alone and coated with NP plus a high ionic strength treatment (0.2 M Na_2SO_4). NPs were clearly detected in both samples, and a slightly "patchier" cover was observed due to NP aggregation after the 0.2M Na_2SO_4 treatment (Figure 6b).

Figure 5c is a histogram of measured height for both samples (*i.e.*, quartz slides with and without ionic strength treatment). The relative height of each particle was measured with the AFM and NanoScope section analysis, indicating the topography along the samples from the dark area (no nanoparticle coating) to the highest NP peaks. Because the NP diameter was confirmed by TEM as 199 nm ± 5 nm, any additional height measured with the NanoScope section analysis should represent the separation distance between the particles and quartz surface. For the data in Figure 5c, there is no significant difference ($p<0.05$) between the mean values of height without (244 nm) versus with the ionic strength treatment (239 nm). Therefore, the separation distance between NPs and surface should be randomly distributed on the order of 5 nm to 80 nm. However, the range and distribution of height on the plate after high ionic strength treatment (244 ± 40 nm) was statistically different ($p>0.05$) than the non-ionic strength treated sample (239 ± 27 nm). Hence, without ionic strength treatment there is a higher frequency for nanoparticles to be in the mean height range from the substrate, while after treatment the distribution shifted so that some particles were located closer to the surface while others were farther away. These

results agree with previous work on other particles such as gold,[35] alumina,[36] or titanium dioxide;[37] ionic strength will change the minimum interparticle distance for these deposited particles, indicating the nanoparticles were aggregated. As previously discussed, any variation in measured height corresponds to the proximity of nanoparticles to substrate (Figure 3). Hence, treating SEOF with higher ionic strength solutions led to nanoparticles staying closer to the interface, decreasing the separation distance.

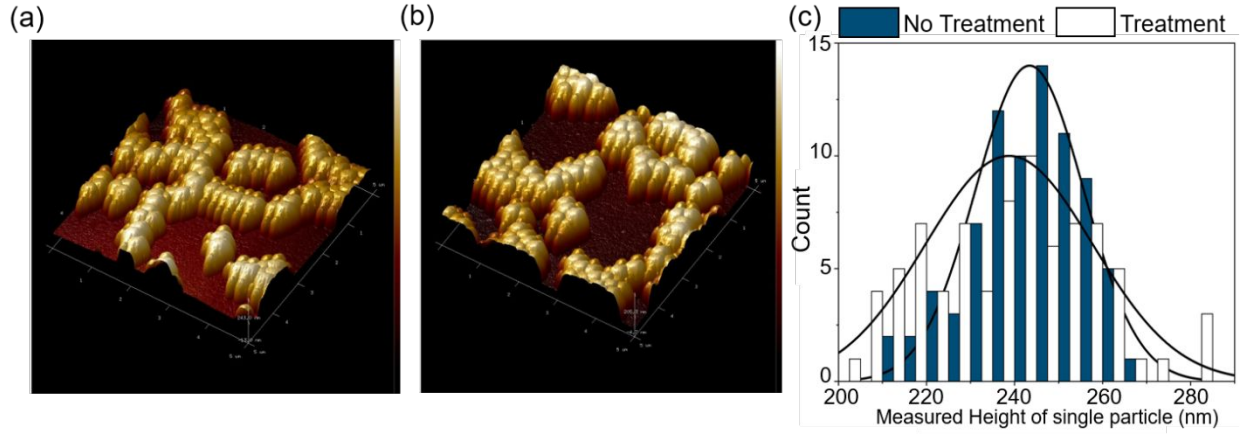

Figure 5 Atomic force microscopy (AFM) images of coated samples (a) without Na_2SO_4 treatment; (b) treated with 0.2 M Na_2SO_4. (c) Histogram of measured height of silica nanoparticles on quartz plate; 80 particles were manually counted for each sample (with and without ionic strength treatment).

When charged particles are immersed in the electrolyte solution (*i.e.*, Na_2SO_4), the ions compress the electrical double layer (EDL) around both NP and optical fiber surfaces.[38] EDL compression lessens the net energy of repulsion between the two surfaces as described mathematically by Derjaguin–Landau–Verwey–Overbeek (DLVO) theory.[39] DLVO theory describes the net energies of interaction between to surfaces as a function of h. Using estimates of Hamaker

constants for silica and zeta potential for negatively charged silica surface and positively charged aminated silica NP,[40] the net energies of interaction were estimated for our system under varying ionic strengths (See Supporting Information and Figures SI.10 and SI.11). In terms of either NP-surface or NP-NP interactions, increasing ionic strength reduced repulsive potential across all separation distances, as expected. Consistent with AFM data illustrated in Figure 5c, increasing ionic strength led to both NP-aggregation and formation of patchy NP aggregates with shorter separation distances on the surface of the optical fiber. Overall, our experimental results support our previous modeling results that separation distance significantly affects side-emitted light scattering.

To further explore NP aggregation effects, optical profilometry was used to measure surface roughness on the optical fiber throughout SEOF fabrication. Figure 6a shows optical profilometer images. The pristine SEOF has a smooth surface and a calculated surface roughness of 4.92 ± 0.07 nm. The SEOF coated with 200 nm NP (no further Na_2SO_4 treatment) had much higher calculated surface roughness of 268 ± 10 nm. Roughness was 399 ± 13 nm after a subsequent ionic strength treatment (0.2M Na_2SO_4). The roughness and optical profilometer images show a similar "patchy" collection of NPs on the surface, with more frequent NP aggregates (Figure 6c) present after ionic strength treatment. These interpretations are consistent with AFM results. Collectively, the experimental results demonstrate that ionic strength treatment 1) results in NP on SEOF surfaces having separation distances on the order of 5 to 80 nm and 2) increases SEOF surface roughness. Evidence from physical measurements (Figure 2) and first-principle models (Figure 3) demonstrates that integrating ionic-strength treatment into SEOF synthesis increases contribution of evanescent wave energy towards side-emitted light.

Thus, modulating separation distance through ionic strength treatment could serve as a design tool to create SEOFs with differing extents of side-emitted light.

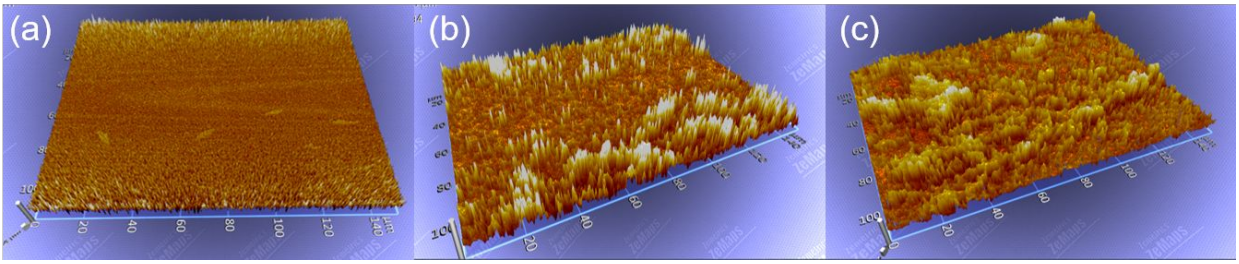

Figure 6 Representative optical profilometry images of (a) pristine optical fiber; (b) optical fiber coated with 200 nm silica sphere nanoparticles; (c) optical fiber coated with 200 nm silica sphere nanoparticles and treated with 0.2M Na_2SO_4. Calculated surface roughness values from triplicate measurements were 4.92 ± 0.07, 268 ± 10, and 399 ± 13 nm, respectively.

As described above, we observed that ionic strength treatment not only increased side emission (*e.g.*, Figure 2) but also led to NP aggregation on fiber surfaces and "patches" of NP aggregates. A hypothesis is that additional dip-coating cycles after a relatively dense NP loading will not increase scattering but only change the particle distribution. To better understand the connection between NP coverage and separation distance, the modelling scattering flux was varied by NP coverage from 0 to 100% (Figure 7). The NP coverage is defined as the ratio of area covered with NPs to the overall fiber surface area. Modeling revealed a sharp increase of total light intensity, as well as inhomogeneity of light distribution, with the increasing coverage. This finding was consistent with the previous work that tunable photocatalyst coverage changes the reaction performance by varying photon use.[41, 42] However, once the NP surface area coverage reached 70%, limited additional side emission (*i.e.,* <10% overall light increase) results from a relatively short separation distance (*e.g.*, <20 nm) (Figure 5a and 5b). Overall, the model

suggests that the separation distance (h) is more influential than NP coverage on the amount of side-emitted light (*i.e.*, intensity). Perhaps equally as important is that NP aggregation due to ionic strength treatment is not detrimental to producing side-emitted light.

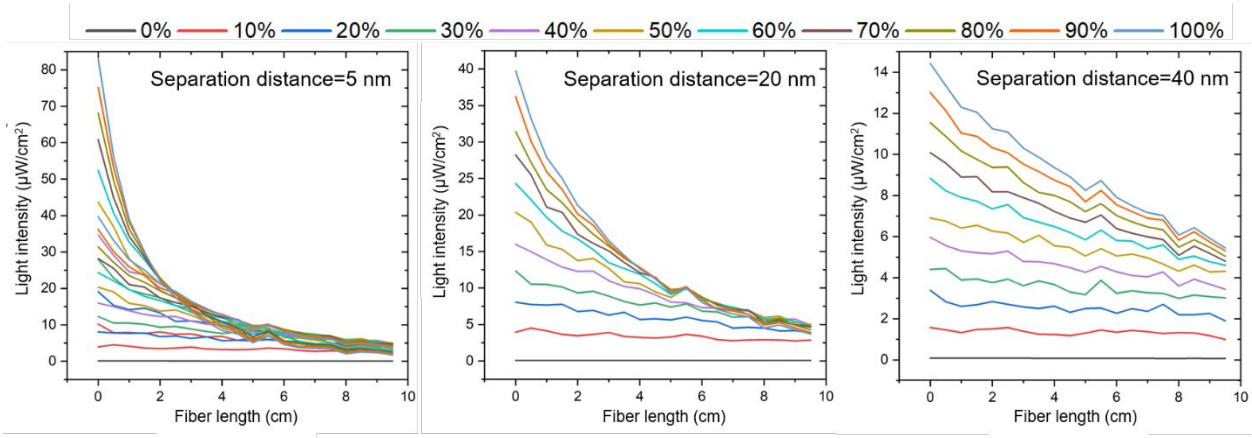

Figure 7 UV-C light irradiance from a mathematical model. NP coverages ranging from no nanoparticles (0% coverage) to 100% coverage on the SEOF surface. Separation distance was set at 5 nm (left), 20 nm (middle), or 40 nm (right). Note that the y-axis is different.

Towards uniform light emission along the length of SEOFs

Knowledge gained from this study provides evidence that high ionic strength solutions could regulate the light scattering along the optical fiber by controlling the proximity between NPs and the fiber surface. Hence, applying different ionic strength to different length-segments of SEOF may make it possible to generate a more uniform light distribution.

Figure 8a shows the scattering flux along the length of two longer SEOFs. The control SEOF without ionic strength treatment shows an exponential decrease of light scattering from proximal end to terminal end. The second SEOF was treated by gradually increasing ionic strength along its length (submerged into a 0.02 M, 0.05 M, 0.10 M, and 0.15 M sodium sulfate solution at 6

cm, 12 cm, 18 cm, 24 cm, respectively) with the concept of achieving variable *h* along the SEOF length. Figure 8b schematically illustrates the mechanism of enhanced side emission associated with increasing ionic strength treatment and tunability of NP separation distance from the surface of the optical fiber. Higher *h* near the LED (*x*=0) would allow less light to be side-emitted because of less interaction with the evanescent waves, whereas lower *h* moving along the axial length would result in a larger percentage of the evanescent wave energy interacting the NP on the SEOF surface and side-emitting more light. Data in Figure 8a were fit with natural logarithm functions (Figure SI.12) to calculate the α based on Equation 2. Without ionic strength treatment, the emitted light intensity will gradually decrease along the fiber (α=0.11), reaching < 10 $\mu W/cm^2$ at a distance of 10 cm. Relatively low light scattering was observed beyond 15 cm which led to a higher irradiation time required to achieve a given UV dose along the SEOF. At the terminal end, some light was reflected back in the opposite direction, creating a second "input light source" at the distal end that increased the light intensity. Varying the ionic strength made the side-emitted light intensity more uniform along the length of the SEOF. At 6 cm from the LED, the light intensity distribution was similar with (α =0.12) versus without (α=0.11) ionic strength treatment and was most likely controlled by refractive light interactions. However, at longer distances (6–12 cm, 12–18 cm, 18–24 cm, and 24–30 cm), compressing the *h* by using different ionic strength led to approximately a 3*x* increase in light intensity. Overall, the fitted scattering coefficient of variable-treated SEOF was 0.047, which is much lower than that of the non-treated SEOF (0.11) (Figure SI.9).

To mathematically evaluate the uniformity of light emission along the SEOF under different treatments, the UC of each fiber was compared. In Figure 8a, the UC for the 30 cm control fiber

was 0.13 and was much lower than unity. The exponential decrease in side-emitted light is caused by 1) the highest light intensity being at the SEOF end nearest the LED, 2) energy available for side-emission along the SEOF decreasing as light is emitted, and 3) a relatively constant *h* value resulting in similar extent of interaction with the evanescent waves. However, the 30 cm SEOF treated with the variable ionic strengths shown in Figure 8a has a 4*x* improvement in UC to 0.52, signifying a transition to more uniform side-emitted light intensity along the length of the fiber. This UC value demonstrates a significantly higher uniformity coefficient for light distribution compared to our prior work with SiO_2 (UC = 0.15) and estimates from TiO_2 coated optical fibers (0.04 < UC < 0.15) using UV-A and longer wavelengths for photocatalytic applications (see Table SI.5). Further optimization of this "ionic strength variation" is being integrated into scaled-up SEOF production and is clearly a function of the desired overall SEOF length and inlet LED light intensity. Insights and calculations gained from experiments and models can now be applied to improve UC along any length of fiber, which extends the useable length that can achieve the intensity necessary to mitigate biofilm growth (*i.e.*, > 2 μW/cm^2).

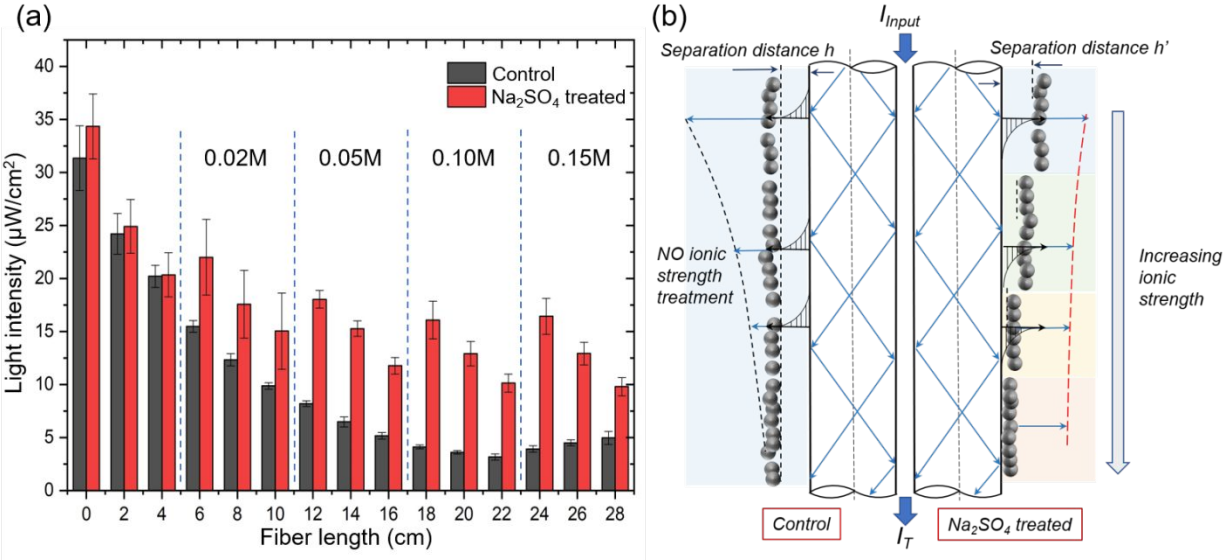

Figure 8 (a) Scattering flux along 30 cm SEOF treated with a series of high ionic strengths. (b) Schematic of the influence of ionic strength on improved side scattering from SEOF. The dip-coating method was applied to different sections along the optical fiber. The fiber at 6 cm, 12 cm, 18 cm, and 24 cm was submerged in 0.02 M, 0.05 M, 0.10 M, and 0.15 M sodium sulfate solution, respectively. Control represents the side emission of NP-coated optical fiber without ionic strength treatment. The standard deviation for triplicate independent optical fibers are illustrated as error bars.

Summary and Conclusions

This paper illustrates that treating NP-coated optical fiber with high ionic strength solution increased the total scattering light intensity and modulated the light distribution (*e.g.*, α). The positive correlation between light intensity and ionic strength could be attributed to the change in separation distance. First-principle modelling results showed that separation distances of 0 to 30 nm strongly influenced the side emission. The smaller separation distance increased scattering flux ratio by up to 10*x* because of the excitation's contributions provided by evanescent wave energy. Optical microscope measurements demonstrated a higher frequency of closer distances between NPs and the optical fiber after ionic strength treatment. Controlling the proximity by varying ionic strength treatment could increase the effective length of optical fiber and fabricate a more uniform SEOF, with a 4*x* improvement in UC over a 30 cm fiber. Modifications described herein could make possible to fabricate longer optical fibers with more even light distribution for water treatment. Using the insights and modeling capabilities developed herein, future work will explore the performance and flexibility of thinner diameter SEOFs and using them to bundle of multiple SEOFs. Ongoing research (e.g., using lenses to collimate light) is

addressing how to increase the percentage of light emitted from the LED into the optical fiber. Ultimately we hope to use SEOFs to deliver germicidal UV-C light from LEDs into piping/tubing, water treatment processes (*e.g.*, membranes), and water storage tanks associated with *legionella* risks.

Acknowledgments

This work was partially funded by the National Science Foundation Nanosystems Engineering Research Center for Nanotechnology-Enabled Water Treatment (EEC-1449500), Hong Kong Research Grants Council (Project No. 16202219), and NASA (80NSSC19C0564). We would like to acknowledge the Eyring Materials Center at Arizona State University supported in part by the National Science Foundation (ECCS-1542160). Laurel Passantino provided technical editing.

References

1. J. Chen, S. Loeb and J.-H. Kim, LED revolution: fundamentals and prospects for UV disinfection applications, *Environmental Science: Water Research & Technology*, 2017, **3**, 188-202.
2. K. G. Linden, N. Hull and V. Speight, Thinking Outside the Treatment Plant: UV for Water Distribution System Disinfection, *Accounts of Chemical Research*, 2019, **52**, 1226-1233.
3. M. Lanzarini-Lopes, B. Cruz, S. Garcia-Segura, A. Alum, M. Abbaszadegan and P. Westerhoff, Nanoparticle and Transparent Polymer Coatings Enable UV-C Side-Emission Optical Fibers for Inactivation of in Water, *Environmental science & technology*, 2019, **53**, 10880.
4. N. M. Hull, W. H. Herold and K. G. Linden, UV LED water disinfection: Validation and small system demonstration study, *AWWA Water Science*, 2019, **1**, e1148.
5. P. Jarvis, O. Autin, E. H. Goslan and F. Hassard, Application of Ultraviolet Light-Emitting Diodes (UV-LED) to Full-Scale Drinking-Water Disinfection, *Water*, 2019, **11**.
6. L. Lin, H. Wang, H. Luo and P. Xu, Enhanced photocatalysis using side-glowing optical fibers coated with Fe-doped TiO2 nanocomposite thin films, *Journal of Photochemistry and Photobiology A: Chemistry*, 2015, **307-308**, 88-98.
7. M. E. Potter, D. J. Stewart, A. E. Oakley, R. P. Boardman, T. Bradley, P. J. A. Sazio and R. Raja, Combining Photocatalysis and Optical Fiber Technology toward Improved

Microreactor Design for Hydrogen Generation with Metallic Nanoparticles, *ACS Photonics*, 2020, **7**, 714-722.
8. T. Matsunaga and M. Okochi, TiO2-Mediated Photochemical Disinfection of Escherichia coli Using Optical Fibers, *Environmental Science & Technology*, 1995, **29**, 501-505.
9. G. Lu, C. Li, Y. Zheng, Q. Zhang, J. Peng and M. Fu, A novel fiber optical device for ultraviolet disinfection of water, *Journal of Photochemistry and Photobiology B: Biology*, 2008, **92**, 42-46.
10. T.-D. Pham and B.-K. Lee, Disinfection of Staphylococcus aureus in indoor aerosols using Cu–TiO2 deposited on glass fiber under visible light irradiation, *Journal of Photochemistry and Photobiology A: Chemistry*, 2015, **307-308**, 16-22.
11. L. Jiao, N. Zhong, X. Zhao, S. Ma, X. Fu and D. Dong, Recent advances in fiber-optic evanescent wave sensors for monitoring organic and inorganic pollutants in water, *TrAC Trends in Analytical Chemistry*, 2020, **127**, 115892.
12. G. Wandermur, D. Rodrigues, R. Allil, V. Queiroz, R. Peixoto, M. Werneck and M. Miguel, Plastic optical fiber-based biosensor platform for rapid cell detection, *Biosensors and Bioelectronics*, 2014, **54**, 661-666.
13. X. Hu, K. Yang and C. Zhang, Optimization of Preparation Conditions for Side-Emitting Polymer Optical Fibers Using Response Surface Methodology, *Polymers*, 2020, **12**, 3062.
14. E. G. Rawson, Analysis of Scattering from Fiber Waveguides with Irregular CoreSurfaces, *Appl. Opt.*, 1974, **13**, 2370-2377.
15. M. Lanzarini-Lopes, Z. Zhao, F. Perreault, S. Garcia-Segura and P. Westerhoff, Germicidal glowsticks: Side-emitting optical fibers inhibit Pseudomonas aeruginosa and Escherichia coli on surfaces, *Water Research*, 2020, **184**, 116191.
16. A. Reupert, M. Heck, S. Nolte and L. Wondraczek, Side-emission properties of femtosecond laser induced scattering centers in optical fibers, *Opt. Mater. Express*, 2019, **9**, 2497-2510.
17. L. Ling, H. Tugaoen, J. Brame, S. Sinha, C. Li, J. Schoepf, K. Hristovski, J.-H. Kim, C. Shang and P. Westerhoff, Coupling Light Emitting Diodes with Photocatalyst-Coated Optical Fibers Improves Quantum Yield of Pollutant Oxidation, *Environmental Science & Technology*, 2017, **51**, 13319-13326.
18. R. El Abdi, A. Rujinsky, C. Borda, I. Severin and M. Poulain, New method for strength improvement of silica optical fibers, *Optics and Lasers in Engineering*, 2008, **46**, 222-229.
19. M. Lanzarini-Lopes, S. Garcia-Segura, K. Hristovski, M. Messerly, A. J. Simon and P. Westerhoff, Particle-modified polymeric cladding on glass optical fibers enhances radial light scattering, *J. Opt. Soc. Am. B*, 2019, **36**, 1623-1628.
20. H. Chew, D.-S. Wang and M. Kerker, Elastic scattering of evanescent electromagnetic waves, *Appl. Opt.*, 1979, **18**, 2679-2687.
21. W. C. Wang, B. Zhou, S. H. Xu, Z. M. Yang and Q. Y. Zhang, Recent advances in soft optical glass fiber and fiber lasers, *Progress in Materials Science*, 2019, **101**, 90-171.
22. T. Azargoshasb, H. A. Navid, R. Parvizi and H. Heidari, Evanescent Wave Optical Trapping and Sensing on Polymer Optical Fibers for Ultra-Trace Detection of Glucose, *ACS Omega*, 2020, **5**, 22046-22056.

23. M. Oheim, A. Salomon, A. Weissman, M. Brunstein and U. Becherer, Calibrating Evanescent-Wave Penetration Depths for Biological TIRF Microscopy, *Biophysical Journal*, 2019, **117**, 795-809.
24. H. Zhang, Z. Chen and X. Wu, Scattering of evanescent wave generated by total reflection, *Journal of Quantitative Spectroscopy and Radiative Transfer*, 2021, **260**, 107480.
25. W. Wang and Y. Ku, The light transmission and distribution in an optical fiber coated with TiO2 particles, *Chemosphere*, 2003, **50**, 999-1006.
26. C. F. Bohren and D. R. Huffman, *Absorption and scattering of light by small particles*, John Wiley & Sons, 2008.
27. J. Zhang, Y. Fu, M. H. Chowdhury and J. R. Lakowicz, Enhanced Förster Resonance Energy Transfer on Single Metal Particle. 2. Dependence on Donor−Acceptor Separation Distance, Particle Size, and Distance from Metal Surface, *The Journal of Physical Chemistry C*, 2007, **111**, 11784-11792.
28. S. Li, T. Zhang, Z. Zhu, N. Gao and Q.-H. Xu, Lighting up the gold nanoparticles quenched fluorescence by silver nanoparticles: a separation distance study, *RSC Advances*, 2016, **6**, 58566-58572.
29. G. Morris, M. R. Pursell, S. J. Neethling and J. J. Cilliers, The effect of particle hydrophobicity, separation distance and packing patterns on the stability of a thin film, *Journal of Colloid and Interface Science*, 2008, **327**, 138-144.
30. Y. Du, in *Encyclopedia of Remote Sensing*, ed. E. G. Njoku, Springer New York, New York, NY, 2014, DOI: 10.1007/978-0-387-36699-9_41, pp. 150-158.
31. J. W. Swan and J. F. Brady, Anisotropic diffusion in confined colloidal dispersions: The evanescent diffusivity, *The Journal of Chemical Physics*, 2011, **135**, 014701.
32. G. Bao and T. Van, Modeling of Evanescent Energy in Optical Fibers, *Journal of Computational Physics*, 2000, **161**, 700-717.
33. F. Wang, C. H. Chon and D. Li, Particle separation by a moving air–liquid interface in a microchannel, *Journal of Colloid and Interface Science*, 2010, **352**, 580-584.
34. H. Matsuoka, Evanescent Wave Light Scattering A Fusion of the Evanescent Wave and Light Scattering Techniques to the Study of Colloids and Polymers Near the Interface, *Macromolecular Rapid Communications*, 2001, **22**, 51-67.
35. E. S. Kooij, E. A. M. Brouwer, H. Wormeester and B. Poelsema, Ionic Strength Mediated Self-Organization of Gold Nanocrystals: An AFM Study, *Langmuir*, 2002, **18**, 7677-7682.
36. A. E. Bayat, R. Junin, F. D. Ghadikolaei and A. Piroozian, Transport and aggregation of Al2O3 nanoparticles through saturated limestone under high ionic strength conditions: measurements and mechanisms, *Journal of Nanoparticle Research*, 2014, **16**, 1-12.
37. M. Zhu, H. Wang, A. A. Keller, T. Wang and F. Li, The effect of humic acid on the aggregation of titanium dioxide nanoparticles under different pH and ionic strengths, *Science of the Total Environment*, 2014, **487**, 375-380.
38. G. Trefalt, S. H. Behrens and M. Borkovec, Charge Regulation in the Electrical Double Layer: Ion Adsorption and Surface Interactions, *Langmuir*, 2016, **32**, 380-400.
39. R. Hogg, T. W. Healy and D. W. Fuerstenau, Mutual coagulation of colloidal dispersions, *Transactions of the Faraday Society*, 1966, **62**, 1638-1651.
40. L. Bergström, Hamaker constants of inorganic materials, *Advances in Colloid and Interface Science*, 1997, **70**, 125-169.

41. S. Mukhopadhyay, D. Maiti, S. Chatterjee, P. S. Devi and G. Suresh Kumar, Design and application of Au decorated ZnO/TiO2 as a stable photocatalyst for wide spectral coverage, *Physical Chemistry Chemical Physics*, 2016, **18**, 31622-31633.
42. C. Li, S. Wang, T. Wang, Y. Wei, P. Zhang and J. Gong, Photocatalysts: Monoclinic Porous BiVO4 Networks Decorated by Discrete g-C3N4 Nano-Islands with Tunable Coverage for Highly Efficient Photocatalysis, *Small*, 2014, **10**, 2782-2782.